AC electrothermal enhancement of heterogeneous assays in microfluidics†

Hope C. Feldman, Marin Sigurdson and Carl D. Meinhart*

Received 4th May 2007, Accepted 25th July 2007
First published as an Advance Article on the web 10th August 2007
DOI: 10.1039/b706745c

AC-driven electrothermal flow is used to enhance the temporal performance of heterogeneous immuno-sensors in microfluidic systems by nearly an order of magnitude. AC electrokinetic forces are used to generate electrothermal flow, which in turn produces a circular stirring fluid motion that enhances the transport of diffusion-limited proteins. This provides more binding opportunities between suspended antigens and wall-immobilized antibodies. We investigate experimentally the effectiveness of electrothermal stirring, using a biotin–streptavidin heterogeneous assay, in which biotin is immobilized, and fluorescently-labeled streptavidin is suspended in a high conductivity buffer (σ = 1.0 S m^{-1}). Microfabricated electrodes were integrated within a microwell and driven at a frequency of f = 200 kHz and 10 V_{rms}. Fluorescent intensity measurements show that for a five minute assay, electrothermal stirring increases the binding rate by a factor of almost nine. Similar binding improvement was measured for longer assays, up to fifteen minutes. The electrothermal enhancement of this assay was modeled numerically and agrees with experimental binding rates. The measured fluid velocity of 22 $\pm$ 2 μm s^{-1} was significantly lower than that predicted by the numerical model, 1.1 mm s^{-1}, but nevertheless shows the same fourth power dependence on applied potential. The results demonstrate the ability for electrothermal stirring to reliably improve the response time and sensitivity within a given time limit for microfluidic diffusion-limited sensors.

1 Introduction

1.1 Immunoassay

An immunoassay is a highly selective and sensitive analytical detection technique, involving specific antigen–antibody binding reactions, used for biological and chemical analysis with various applications in infectious disease diagnostics, immunology, detection of biological warfare agents, and environmental diagnostics. Conventional immunoassays, such as microarrays or enzyme-linked immunosorbent assays (ELISA) using microtiter plates, can be limited in response time and sensitivity by diffusion limitations of the antigen to the immobilized antibody.[1] This leads to long incubation times, ranging from minutes to several hours, and significantly limits throughput. For time-critical immunoassay applications, such as biowarfare detection[2] and point-of-care diagnostics,[3] these challenges need to be addressed. In bench-top clinical laboratories, achieving high-throughput can be met through the use of robotic techniques and larger array formats.[4] Additionally, recent work has shown that using multiple fluorescent dyes (FLISA)[5] or surface plasmon resonance can increase throughput.[6]

Smaller length scale systems, such as microarrays and lab-on-a-chip sensors, can innately improve temporal response over traditional assays,[3,7] but many of these devices are still diffusion limited. Research has been conducted to increase throughput in these microsystems, such as microfluidic networks (μFN)[8] and microdilutor networks (μDN)[9] for simplified assay preparation, parallelization using miniaturized micromosaic immunoassays (μMIA)[10,11] or multiple analyte assays.[12,13] Although these techniques contribute to improving throughput, they do not directly impact the problem of long incubation times due to diffusion limitations of the analyte.

Most relevant is the technique proposed by Sigurdson *et al.*[14] to use AC electrothermal flow to augment transport of diffusion-limited reactions. The study modeled numerically the influence of electrothermal flow on a first order protein–ligand reaction and demonstrated the ability of electrothermal stirring to increase binding by a factor of seven within a few minutes using 6 V_{rms} applied potential. Additionally, it was emphasized that electrothermal stirring is most effective for high Damköhler numbers (>100), where the Damköhler number Da is the ratio of reaction velocity ($k_{on}R_T$) to diffusion velocity (D/h).[15]

In the current work, we investigate experimentally electrothermal microstirring binding enhancement using a biotin–streptavidin assay (Damköhler number $\approx$1000). Biotin is immobilized on the bottom of a microwell device and streptavidin is suspended in a high conductivity buffer. We chose this particular protein–ligand system because it has a strong non-covalent biological interaction[16,17] and serves as a paradigm for providing the basis for establishing new technologies in the fields of immunology, medical diagnostics, biochemistry, and cell biology.[18] Therefore, it is a reliable system to investigate electrothermal microstirring.

1.2 AC electrokinetics

Electrokinetics is the study of bulk fluid and/or particle motion resulting from externally applied electric fields.

Department of Mechanical Engineering, University of California, Santa Barbara, CA, 93106, USA. E-mail: meinhart@engr.ucsb.edu; Fax: +1 (805) 893-8651; Tel: +1 (805) 893-4563
† Electronic supplementary information (ESI) available: Velocity and binding results discussion. See DOI: 10.1039/b706745c

Microfabricated electrodes provide a means to non-invasively generate fluid motion and manipulate particles, such as proteins and cells within lab on chip devices. AC electrokinetics encompasses three phenomena: dielectrophoresis (DEP), which allows for particle manipulation, and AC electroosmosis (ACEO) and electrothermal flow (ETF), which cause fluid motion.[19] DEP has been exploited to separate and concentrate DNA, remove cancer cells from blood, purify biosamples, and manipulate submicron particles.[19–25] ACEO has been used for pumping low conductivity fluids.[22,26–30] Because ACEO relies on the formation of a thick double layer, it is not effective in fluids with high electrical conductivities (*i.e.* 1.0 S m^{-1}), such as biological fluids and many reaction buffers, which limits its utility.

1.3 Electrothermal flow

In contrast, ETF is very effective in higher conductivity fluids, and therefore is useful for microstirring biological fluids and enhancing transport of proteins within immunoassays. When an electric field passes through a buffer solution, Joule heating of the solution produces a temperature field according to the energy balance

$$\rho C_p \frac{\partial T}{\partial t} = k\nabla^2 T + \sigma E^2 \quad (1)$$

where T is temperature, E is the magnitude of the electric field, k and σ are the thermal and electrical conductivities, ρ is the mass density, and C_p is the specific heat (at constant pressure). In the steady state, this balance reveals a quadratic dependence of temperature on electric field magnitude.

Gradients in temperature produce gradients in electrical permittivity and conductivity in the fluid. For water, the dependence of electrical conductivity on temperature is $(1/\sigma)(\partial\sigma/\partial T) = +2\%$, and the dependence of electrical permittivity on temperature is $(1/\varepsilon)(\partial\varepsilon/\partial T) = -0.4\%$ per degree Kelvin.[31] These variations in electric properties produce gradients in charge density and perturb the electric field. Assuming the perturbed electric field is much smaller than the applied electric field, and that the advection of electric charge is small compared to conduction, the time-averaged electrothermal force per unit volume for a non-dispersive fluid can be written as[19]

$$\vec{F}_{ET} = -0.5\left[\left(\frac{\nabla\sigma}{\sigma} - \frac{\nabla\varepsilon}{\varepsilon}\right)\cdot\vec{E}\frac{\varepsilon\vec{E}}{1+(\omega\tau)^2} + 0.5\left|\vec{E}\right|^2\nabla\varepsilon\right] \quad (2)$$

where $\tau = \varepsilon\,\sigma^{-1}$ is the charge relaxation time of the fluid medium, and the incremental temperature-dependent changes are

$$\nabla\varepsilon = \left(\frac{\partial\varepsilon}{\partial T}\right)\nabla T,\ \nabla\sigma = \left(\frac{\partial\sigma}{\partial T}\right)\nabla T \quad (3)$$

The first term on the right hand side of eqn (2) is the Coulomb force, and is dominant at low frequencies. The second term is the dielectric force, and is dominant at high frequencies. The crossover frequency scales inversely with the charge relaxation time of the fluid.[19] For example, an aqueous solution with high conductivity σ = 1.0 S m^{-1} has a crossover frequency around 200 MHz.

Well below the crossover frequency ($\omega \ll \tau$), the electrothermal force is dominated by the first term in eqn (2) and scales according to

$$\vec{F}_{ET} \sim \left(\nabla T\cdot\vec{E}\right)\vec{E} \quad (4)$$

Since the temperature scales with E^2, this relation reveals a 4th power dependence of electrothermal force on E, meaning a small increase in applied potential can result in a large increase in velocity, rendering this flow, in theory, easy to magnify. Additionally, eqn (2) shows the heating increases with the solution electrical conductivity, making these physics particularly important for higher conductivity solutions, *e.g.* physiological fluids and buffer solutions.

As explicitly shown in Sigurdson *et al.*,[14] the circulating flow will replenish the depleted region surrounding the functionalized surface and bring more analyte to bind with the antibodies at a faster rate. ETF has the advantage of simple implementation and reliability since it is free of moving parts. Additionally, ETF can operate with low voltages and high frequency, which is conducive to portability, low cost and avoids electrolysis.

2 Methods and materials: experimental

Electrothermal stirring device

The electrothermal stirring devices were fabricated on a silicon substrate by depositing a 200 nm silicon dioxide isolation layer and parallel titanium–gold–titanium electrodes (Fig. 1b). The electrodes (100 Å Ti–1000 Å Au–100 Å Ti) are 9 mm long and are separated by 60 μm gaps. Although there are four parallel electrodes, only the center two electrodes were used in this application.

Biotinylation

Each device was cleaned *via* sonication in acetone for 5 min, followed by 100% ethanol for 5 min. The devices were then surface modified with an amino-silane monolayer (Fig. 1a). Each device was immersed in a 2% v/v solution of (3-aminopropyl) trimethoxysilane (APTMS) (Gelest, Morrisville, PA, USA) in ethanol for 1 h.[32,33] This step is extremely sensitive to water and was therefore performed in a humidity-controlled cleanroom. Each device was thoroughly rinsed with ethanol, lightly rinsed with deionized (DI) water, and then dried with nitrogen. The silane-treated devices were biotinylated with a 10 mM solution of sulfosuccinimidyl 2-(biotinamido)-ethyl-1,3-dithiopropionate (NHS-SS-Biotin) (Pierce Biotechnology, Rockford, IL, USA) in 0.1 M phosphate buffer (PB) aqueous solution (pH 7.8; PB is a lab manufactured stock solution of 0.1 M $NaH_2PO_4{\cdot}H_2O$ added to 0.1 M $Na_2HPO_4{\cdot}7H_2O$ until the pH reached 7.4; next, NaOH was added until the pH reached 7.8). A 5 μL drop of biotin solution (~1.5 mm in diameter) was micropipetted onto the center of the device, and left for 45 min.[32,33] Each device was rinsed with DI water and dried with nitrogen.

Temperature gradient control

Electrothermal motion requires a sufficient temperature gradient within the fluid. In order to maintain this gradient

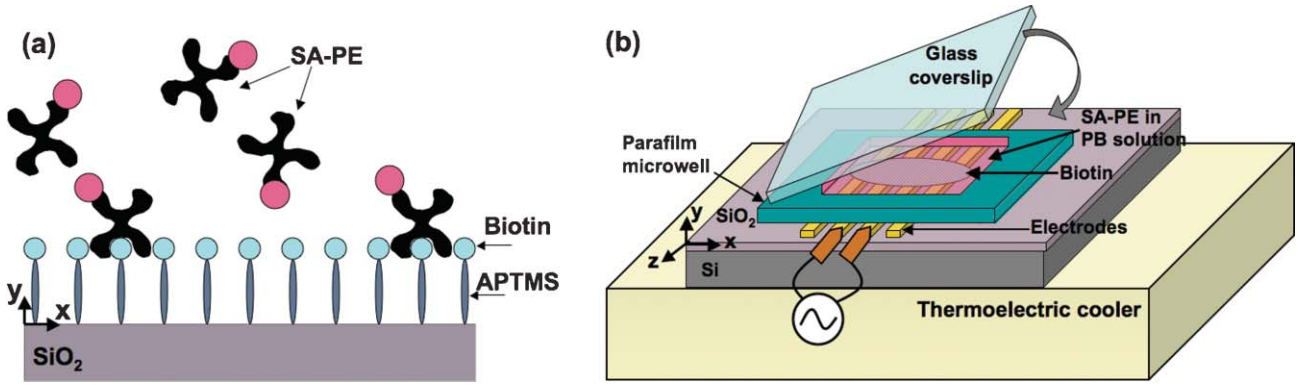

Fig. 1 Electrothermally enhanced biotin–streptavidin heterogeneous immunoassay schematics (not to scale). (a) APTMS functionalized surface, immobilized biotin, and suspended fluorescently labeled streptavidin (SA-PE) in buffer. (b) Experimental set-up of heterogeneous immunoassay in concert with the electrothermal device. The silicon substrate is isolated with a silicon dioxide layer from Ti–Au–Ti electrodes separated by 60 μm gaps. The device is treated with APTMS for biotin immobilization, which is micropipetted in the center of the device. The device sits on a thermoelectric cooler (TEC) maintained at 20 °C and a parafilm cutout forms the microcavity 165 μm ± 30 μm deep, and phosphate buffer (PB) (σ = 1.0 S m^{-1}) containing fluorescently-labeled streptavidin fills the cavity. A glass cover-slip closes the micro-cavity. The inner two electrodes were driven at a frequency f = 200 kHz with amplitude 10 V_{rms}.

in the presence of Joule heating, a thermoelectric cooler (Tellurex Corporation, Traverse City, MI, USA) was mated to the backside of the silicon base. The thermoelectric cooler (TEC) removes heat from the device and maintains a cool bottom wall. The high thermal conductivity of the device base (Si) is necessary for this heat removal. The TEC was controlled by a PID temperature controller (model 988, Watlow Electric Manufacturing Company, St Louis, MO, USA) and a thermocouple. The temperature was maintained at 20 °C ± 1 °C.

Introduction of fluorescent streptavidin

After the biotinylation of the device, a 5 mm × 5 mm × 165 μm ± 30 μm microcavity was created with a Parafilm M gasket. Parafilm is a thin-hydrocarbon-wax film with adhesive properties, making it suitable for the creation of a leak-free microwell. The microwell was filled with a 1% v/v solution of fluorescently-labeled streptavidin R-phycoerythrin conjugate (SA-PE, fluorescence emission max of ~578 nm) (1 mg mL^{-1}, Molecular Probes, Eugene, OR, USA) in 0.1 M pH 7.4 PB with conductivity σ = 1.0 S m^{-1}. The microcavity was covered with a glass cover slip. The electrodes were connected to a frequency generator *via* miniature copper clips. The electrodes were driven at a frequency f = 200 kHz with an amplitude of 10 V_{rms} for a specified time, ranging from 1–15 minutes (Fig. 1b). The times were determined experimentally in order to reveal the steady state behavior in binding increase.

Epi-fluorescent microscopy

Upon disconnecting the potential, the glass-coverslip and parafilm were removed, and the device was rinsed with 0.1 M pH 7.4 PB, and then dried with nitrogen. This resulted in the bare device with fluorescent streptavidin bound to the biotin spot. The biotin–streptavidin binding was evaluated using an epi-flourescent microscope (Nikon E600FN) with a 10× objective lens (NA = 0.25), a mercury arc lamp, and a filter cube optimum for phycoerytherin (Chroma Technology, Rockingham, VT, USA). The images of the biotin–streptavidin binding, including both fluorescent spot and background areas, were captured with a cooled CCD camera (PIVcam 13-8; 1024 × 1024; TSI Inc., Shoreview, MN, USA).

Particle image velocimetry

Fluid velocity was estimated by measuring tracer particle velocity using micro particle image velocimetry (micro-PIV), described in Meinhart *et al.* (1999)[34] and Santiago *et al.* (1998).[35] The 0.1 M, pH 7.4 PB is seeded with 0.7 μm fluorescent polystyrene particles (Duke Scientific, Fremont, CA, USA). The particles are illuminated with a frequency doubled Nd:YAG laser (532 nm) (New Wave Research, Inc., Fremont, CA, USA) and imaged through an epi-fluorescent microscope with a 40× objective (NA = 0.75). Image pairs are recorded with a cooled CCD camera. Image pair temporal separation (Δt) is adjusted between 0.05 and 0.1 s to fit the speed of the flow. Forty image pairs are compared and ensemble averaged using proprietary PIV software to yield a particle velocity-vector field $\boldsymbol{u}(x,z)$, where $\boldsymbol{u}$ = $[u,w]$. Measurements were taken at various x–z planes. Because the electrodes are long, velocity is essentially uniform in the z-direction, and therefore velocity vectors are averaged in the z-direction.

3 Methods: numerical model

3.1 Electrothermal

A numerical model was developed using the COMSOL Multiphysics V3.2 (COMSOL, Inc. Stockholm, Sweden) finite element package.[14] First, the two-dimensional quasi-static potential field is calculated within the fluid, according to Laplace's equation, $\nabla^2 V = 0$. The resulting electric field is given by $E = -\nabla V$. The temperature field (eqn (1)) is then solved for the device (silicon base, oxide isolation layer, fluid, and glass cover). Parafilm walls have low heat capacity and conductivity and are therefore considered insulating boundary

conditions. Metal electrodes, though high k, are thin enough (1200 Å) that they do not significantly affect heat transfer. Because of the scale of the system, convective heat transport is not important and is ignored here. The bottom of the silicon base is maintained at T = 20 °C to match the TEC. The electrothermal force is calculated from eqn (2), and is then used as a forcing term in the Navier–Stokes equations to solve for fluid velocity.

3.2 Binding

We next determine how the ETF affects the binding of a suspended analyte (here, fluorescently tagged streptavidin) to an immobilized receptor (biotin). The convective scalar equation describes the suspended concentration $c(x,y,t)$ of analyte within the microchannel:

$$\frac{\partial c}{\partial t} + \vec{u}\cdot\nabla c = D\nabla^2 c \tag{5}$$

where u is the fluid velocity and D the diffusivity of the analyte. An initial concentration in the cavity c_0 is depleted through binding at the wall. Following the model given by Myszka,[36] the rate of binding at the wall for a first order reaction is $k_{on}c_w(R_T - B)$, where k_{on} is the on rate constant, R_T is the receptor concentration, B is the bound antigen concentration, and $c_w(x)$ is the suspended concentration of antigen along the wall. The rate of dissociation is $k_{off}B$, where k_{off} is the off rate constant. The time rate of change of antigen bound to the immobilized antibodies, $\partial B/\partial t$, is equal to the rate of association minus the rate of dissociation

$$\frac{\partial B}{\partial t} = k_{on}c_w(R_T - B) - k_{off}B \tag{6}$$

The rate of antigen binding to immobilized antibodies must be balanced by the diffusive flux of antigen at the binding surface, y = 0, such that

$$\frac{\partial B}{\partial t} = D\frac{\partial c}{\partial y}\bigg|_{y=0} \tag{7}$$

Eqn (5), (6) and (7) are solved with the following constants: R_T = 3.3 × 10^{-11} M m (*i.e.* 2 × 10^{16} molecules per m^2); k_{on} = 10^6 M^{-1} s^{-1}; k_{off} = 10^{-3} s^{-1}; D = 5 × 10^{-12} m^2 s^{-1}.

4 Results

4.1 Velocity: numerical model and measurements

Electrothermal velocity predicted by the numerical model is shown in Fig. 2. The two electrodes on the cavity bottom are driven with an AC potential of 10 V_{rms} at frequency f = 200 kHz. Joule heating produces a local temperature increase in the fluid of 11.8 K between and above the electrodes. Because of the high thermal conductivity of the silicon base, the temperature excursion on the cavity bottom where the binding reaction occurs is limited to 1.8 K. The temperature gradient results in a conductivity gradient that interacts with the applied field to produce an electrothermal body force on the fluid and the electrothermal flow shown in the figure. Maximum predicted velocity is 1.1 mm s^{-1}.

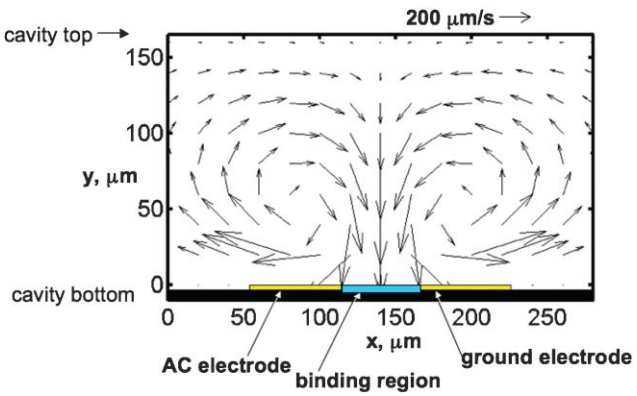

Fig. 2 Numerical model of electrothermal velocity. Two long, parallel electrodes on cavity bottom are driven at 200 kHz; 10 V_{rms}. Maximum electrothermal velocity generated is 1.1 mm s^{-1}, near the inside edges of the electrodes. Cavity sides extend well beyond plotted region.

The experimentally-measured velocity is more than an order of magnitude lower than the simulations. The maximum measured velocity is 22 ± 2 μm s^{-1}. However, the measured velocity field pattern matches the numerically simulated pattern (Fig. 2). In addition, the measured dependence of velocity on voltage agrees with the model. According to eqn (4), the ETF velocity is expected to increase with the fourth power of applied potential. Fig. 3 shows the ETF velocity, estimated from the numerical simulations and measured from the experiments, *versus* applied ac potential in log–log coordinates. The experimental results from five devices indicate that the velocity increases with applied voltage $|\boldsymbol{u}| \sim V^{4.09\pm0.15}$ (see Fig. 3). This suggests that the electrothermal effect is the dominant driving mechanism. The measured velocity is the maximum velocity in the plane located at y = 11 μm.

From Fig. 3, it is clear that the experimentally-measured velocity is more than an order of magnitude lower than the numerical simulations. However, if the effective voltage in the

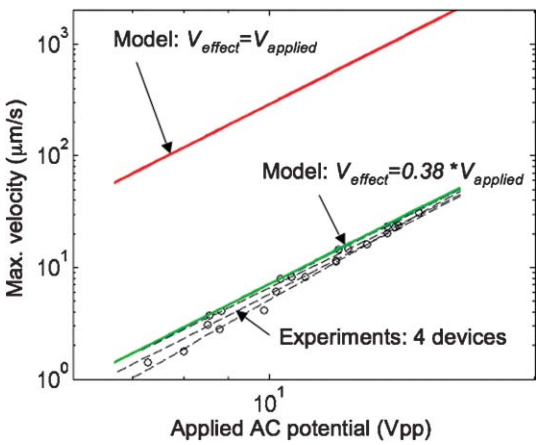

Fig. 3 Electrothermal velocity increases with voltage to the 4th power (numerical simulation; solid line); or to the 4.09 ± 0.15 power (experiment; circles and dashed line). This agreement, despite the vast difference in magnitude, suggests the velocity is electrothermal in origin, but may be driven by a reduced "effective" voltage V_{effect} = $0.38V_{applied}$.

numerical simulations is lowered to 38% of the applied voltage, the simulation velocity is reduced significantly, and agrees closely with the experimentally-measured velocity.

4.2 Heterogeneous binding

4.2.1 Numerical model results. The results from the numerical model demonstrate the enhancing effect of electrothermal stirring on the heterogeneous biotin-streptavidin assay. Fig. 4 shows the streptavidin concentration in a portion of the electrothermal device for 1, 5, and 10 min after sample introduction. The domain extends from the device centerline 1 mm outward across a segment of the immobilized biotin spot. The left side of the figure (inner region) includes an active electrode and illustrates half of the electrothermal circulating fluid pattern, whereas the right side of the figure (outer region) is affected minimally by the stirring motion, and therefore the binding response is similar to that of a passive assay. As time progresses, the near-wall concentration in the outer region becomes depleted and prevents further binding of analyte. However, with the electrothermal stirring on the left side, this depleted concentration is replenished with fresh streptavidin, and thereby improves binding in this region.

4.2.2 Experimental results. The imaged results are shown in Fig. 5. The brighter upper halves of Fig. 5a and Fig. 5b are sections of the biotin spot where fluorescent streptavidin has bound; the lower halves are darker where there was no biotinylation. Non-specific binding causes the background to fluoresce slightly. Because background is accounted for in image processing, it is not detrimental to the experiment. The dark stripes are the microfabricated Ti–Au–Ti electrodes separated by 60 μm gaps. Fig. 5a shows a typical passive or

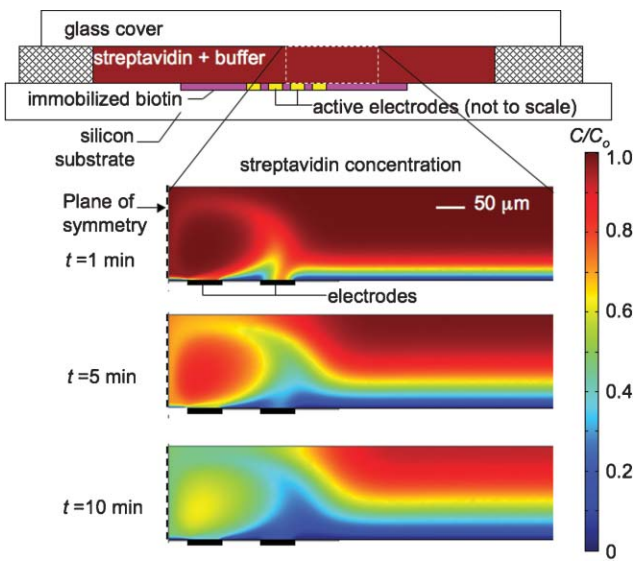

Fig. 4 Numerical model of streptavidin concentration within the microcavity. Concentration is depleted at the wall through specific binding with immobilized biotin. Above the electrodes (left side of figure), electrothermal microstirring circulates this depleted concentration away. Near the electrodes, the binding rate is therefore increased, compared with the static region (right side of figure) where streptavidin can only reach the binding surface through diffusion.

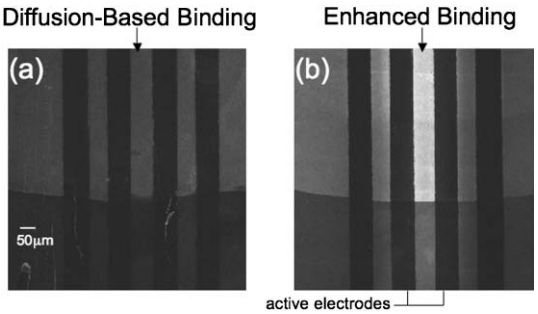

Fig. 5 Electrothermal stirring device viewed through an epi-fluorescent microscope. The dark stripes are the Ti–Au–Ti electrodes and the brighter semi-circle is a section of the biotin spot where fluorescent streptavidin has bound. (a) Passive assay with no electrothermal microstirring. Assay reacted for five minutes. (b) Electrothermally microstirred assay. The inner two electrodes were driven with a potential of 10 V_{rms} and f = 200 kHz for five minutes. The brighter region directly between the excited electrodes indicates a faster reaction. Comparing fluorescent intensities for 17 experiments, we quantify that electrothermal microstirring increases the biotin–streptavidin binding by a factor of 7.8 ± 1.7 over five minutes.

control case assay that was performed with no electrothermal stirring and allowed to react for five minutes. The bright spot where biotin and streptavidin are bound is fairly uniform in fluorescence. Since diffusion is the only transport mechanism in the passive assay, the binding of biotin and streptavidin is relatively homogeneous over the immobilized biotin spot. Fig. 5b is a typical five-minute reaction assay that was enhanced with the electrothermal microstirring. The inner two electrodes were energized with an applied potential of 10 V_{rms} and a frequency of f = 200 kHz for five minutes. The fluorescent spot is brighter, which indicates improved binding and a faster reaction. This effect is most pronounced between the active (center) electrodes where electrothermal flow causes the highest fluid velocity and therefore highest transport rate of streptavidin to the binding surface.

Quantification of the binding between the immobilized biotin and streptavidin was achieved through fluorescent intensity measurements using MATLAB Image Processing Toolbox (Mathworks, Cambridge, MA, USA). Intensity of active (that is, with electrothermal microstirring) and passive assays were compared on the same device for each experiment. The active region was chosen between the active electrodes, whereas the passive region was chosen at a location away from the electrodes where the electrothermal fluid motion is negligible. The binding enhancement factor (BEF) is calculated by

$$\mathrm{BEF} = \frac{\mathrm{active} - \mathrm{background}}{\mathrm{passive} - \mathrm{background}} \tag{8}$$

For each assay duration (1, 3, 5, 7, 9, 15 min), a total of 51 experiments (approximately nine for each time trial) were analyzed to determine experimental repeatability. Fig. 6 shows the average improvement in biotin–streptavidin binding for different assay durations. The improvement factor is 3.0 ± 0.3 for one minute of electrothermal stirring and increases steadily for longer assay times. After five minutes, the increase in

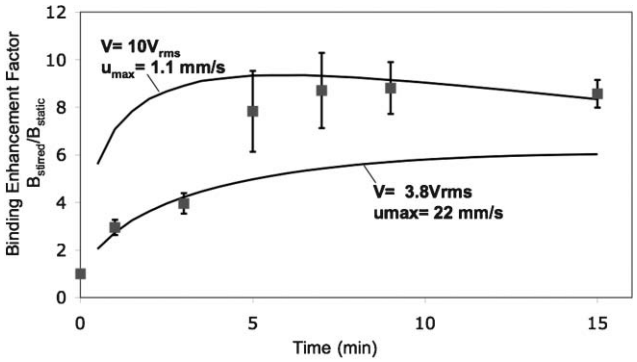

Fig. 6 Binding enhancement factor: binding in electrothermally microstirred region compared with binding in static region ($B_{stirred}/B_{static}$). Squares are experimental measurement; solid lines are numerical model results. Model is run both for actual applied voltage (10 V_{rms}) and for an "effective" voltage (V_{effect} = 0.38 $V_{applied}$) of 3.8 V_{rms}.

binding approaches a maximum value and remains fairly constant through the longest experimental assay of 15 minutes, where the binding improvement is 8.6 $\pm$ 0.6. The binding rate experimental results were repeatable to within $\sim$7% of the mean value, demonstrating the effectiveness and consistency of electrothermal stirring to improve binding rates by nearly an order of magnitude.

5 Discussion

Although the measured velocity varies with voltage to the fourth power, as predicted by the electrothermal model, the magnitude of the measured velocity is over an order of magnitude lower than that predicted by the numerical simulation. We have explored several potential explanations for the low experimentally measured velocity, and have concluded that each is not a significant factor (see ESI†). The explanation for this velocity discrepancy is unclear, and the subject of ongoing investigation.

In order to reconcile the experimental and numerical results, we consider that the ETF is produced by an effective potential $V_{effect} = 0.38 V_{applied}$, such that the simulation velocity produced by V_{effect} matches the experimentally measured velocity. Binding curve simulations (Fig. 6) are shown for both V_{effect} and $V_{applied}$. The experimental results (Fig. 6) appear to agree with the reduced voltage for shorter assay times (1, 3 min), and with the actual voltage model for longer durations. This behavior is not yet well understood, and may be an artifact of the experiment, or the result of experimental variation. It could also be the result of an undetermined transient thermal effect. An increase in temperature gradient with time would lead to a greater microstirring effect and consequently, improve binding more for longer assay times. To determine accurately if there is an increase in the temperature gradient over several minutes, we would need to measure the fluid temperature within fractions of a degree. Presently, no method exists that is capable of measuring fluid temperature within fractions of a degree, and with one micron spatial resolution in the bulk of a microfluidic flow. However, the observed improvement in binding rate is repeatable and consistent to within $\sim$7%. The effect of thermal transients on the binding rate constants was also considered, but determined to be negligible (see ESI†).

Conclusions

Experiments and numerical simulations demonstrate that electrothermal microstirring can be used to improve heterogeneous binding by up to a factor of 9, with only 10 V_{rms} applied voltage. The binding results were repeatable to within 7% for the 51 experiments conducted. The velocity fields measured from experiments and estimated from the numerical simulations have similar velocity patterns but disagree in scale by approximately 1.5 orders of magnitude. Nevertheless, these binding experiments, which were performed in a high conductivity buffer of 1.0 S m^{-1}, reveal the capability for electrothermal motion to effectively manipulate biologically-relevant fluids. This demonstrates that implementing ETF within a diffusion-limited heterogeneous assay can microstir proteins and significantly improve binding rates. The resulting improvement in temporal performance can be used to accelerate existing time-critical immuno-sensors by nearly an order of magnitude.

Acknowledgements

This research was supported by the Institute for Collaborative Biotechnologies through grant DAAD19-03-D-0004 from the U.S. Army Research Office and NSF CTS-0404444. We would like to thank Rohit Karnik from MIT (provided assistance while at UC Berkeley) and Yi Xiao from UCSB for their great help with the biotinylation.

References

1 M. Stenberg and H. Nygren, *J. Immunol. Methods*, 1988, **113**, 3–15.
2 D. N. Stratis-Cullum, G. D. Griffin, J. Mobley, A. A. Vass and V. Dinh, *Anal. Chem.*, 2003, **75**, 275–280.
3 S. K. Sia, V. Linder, B. A. Parviz, A. Siegel and G. M. Whiesides, *Angew. Chem., Int. Ed.*, 2004, **43**, 498–502.
4 D. W. Chan, *Immunoassay Automatization*, Academic Press, San Diego, CA, USA, 1996.
5 E. E. Swartzman, S. J. Miraglia, J. Mellentin-Michelotti, L. Evangelista and P.-M. Yuan, *Anal. Biochem.*, 1999, **271**, 143–151.
6 P. Englebienne, A. Van Hoonacker and M. Verhas, *Spectroscopy*, 2003, **17**(2–3), 255–273.
7 J. S. Rossier and H. H. Girault, *Lab Chip*, 2001, **1**, 153–157.
8 E. Delamarche, A. Bernard, H. Schmid, B. Michel and H. Biebuyck, *Science*, 1997, **276**, 779–781.
9 X. Jiang, J. M. K. Ng, A. D. Stroock, S. K. W. Dertinger and G. M. Whitesides, *J. Am. Chem. Soc.*, 2003, **125**, 5294–5295.
10 A. Bernard, B. Michel and E. Delamarche, *Anal. Chem.*, 2001, **73**, 8–12.
11 M. Wolf, D. Juncker, B. Michel, P. Hunziker and E. Delamarche, *Biosens. Bioelectron.*, 2004, **19**, 1193–1202.
12 C. A. Rowe, L. M. Tender, M. J. Feldstein, J. P. Golden, S. B. Scruggs, B. D. MacCraith, J. J. Cras and F. S. Ligler, *Anal. Chem.*, 1999, **71**, 3846–3852.
13 Y. Gao, G. Hu, F. Y. H. Lin, P. M. Sherman and D. Li, *Biomed. Microdev.*, 2005, **7**(4), 301–312.
14 M. Sigurdson, D. Wang and C. D. Meinhart, *Lab Chip*, 2005, **5**, 1366–1373.
15 W. M. Deen, *Analysis of Transport Phenomena*, Oxford University Press, New York, 1998.
16 N. M. Green, *Adv. Protein Chem.*, 1975, **29**, 85–133.
17 L. Chaiet and F. J. Wolf, *Arch. Biochem. Biophys.*, 1964, **106**, 1–5.
18 E. Bayer and M. Wilcheck, *J. Chromatogr.*, 1990, **510**, 3–11.

19 A. Ramos, H. Morgan, N. G. Green and A. Castellanos, *J. Phys. D: Appl. Phys.*, 1998, **31**, 2338–2353.
20 H. A. Pohl, *Dielectrophoresis: The Behavior of Neutral Matter in Nonuniform Electric Fields*, Cambridge University Press, Cambridge, UK, 1978.
21 P. R. C. Gascoyne and J. Vykoukal, *Electrophoresis*, 2002, **23**, 1973–1983.
22 P. K. Wong, T.-H. Wang, J. Deval and C.-M. Ho, *IEEE/ASME Trans. Mechatron.*, 2004, **9**(2), 366–376.
23 X. Hu, P. Bessette, J. Qian, C. D. Meinhart, P. Daugherty and T. Soh, *Proc. Natl. Acad. Sci. U. S. A.*, 2005, **102**(44), 15757–15761.
24 I. R. Perch-Nielsen, D. D. Bang, C. R. Poulsen, J. El-Ali and A. Wolff, *Lab Chip*, 2003, **3**, 212–216.
25 A. Docoslis, N. Kalogerakis, L. A. Behie and K. V. I. S. Kaler, *Biotechnol. Bioeng.*, 1997, **54**(3), 239–249.
26 A. Adjari, *Phys. Rev. E*, 2000, **61**(1), R45–R48.
27 M. R. Bown and C. D. Meinhart, *Microfluid. Nanofluid.*, 2006, **2**, 513–523.
28 I. Tuval, I. Mezic, F. Bottausci, Y. T. Zhang, N. C. MacDonald and O. Piro, *Phys. Rev. Lett.*, 2005, **95**(236002), 1–4.
29 T. Squires and M. Z. Bazant, *J. Fluid Mech.*, 2004, **509**, 217–252.
30 T. Squires and M. Bazant, *J. Fluid Mech.*, 2006, **560**, 65–101.
31 D. R. Lide, *CRC Handbook of Chemistry and Physics*, CRC Press, New York, 81st edn, 2000.
32 R. Karnik, K. Castelino, C. Duan and A. Majumdar, *Nano Lett.*, 2006, **6**(8), 1735–1740.
33 R. Karnik, K. Castelino, R. Fan, P. Yang and A. Majumdar, *Nano Lett.*, 2005, **5**(9), 1638–1642.
34 C. D. Meinhart, S. T. Wereley and J. G. Santiago, *Exp. Fluids*, 1999, **27**, 414–419.
35 J. G. Santiago, S. T. Werely, C. D. Meinhart, D. J. Beebe and R. J. Adrian, *Exp. Fluids*, 1998, **25**, 316–319.
36 D. G. Myszka, X. He, M. Dembo, T. A. Morton and B. Goldstein, *Biophys. J.*, 1998, **75**(2), 583–594.